# Spectroscopy and Imaging by Laser Excited Terahertz Waves

Masanori HANGYO, Masahiko TANI, Takeshi NAGASHIMA, Hideaki KITAHARA and Hisashi SUMIKURA

*Institute of Laser Engineering, Osaka University, 2-6 Yamadaoka, Suita, Osaka 565-0871, Japan*

(Received 13 December 2006 / Accepted 3 March 2007)

Recently, the technology of generating and detecting terahertz (THz) waves by using ultrashort pulse lasers has made great progress. In this paper, we describe THz spectroscopies and imaging with the intention of applying them to diagnostics of plasmas in the future. After a brief description of the method of generating and detecting THz pulses with a femtosecond laser, the principle of THz time-domain spectroscopy is described. The THz magneto-optical effect measurement system up to the magnetic field of 10 T and down to 5 K is also shown. These systems are used to characterize solid state plasmas in semiconductors. The transmission- and reflection-type imaging systems are described and some examples of measurements are shown. Finally, the application of the THz technology to fusion plasma diagnostics is proposed.



Keywords: terahertz (THz) wave, terahertz time-domain spectroscopy (THz-TDS), femtosecond laser, plasma, imaging, tomography

DOI: 10.1585/pfr.2.S1020

## 1. Introduction

The electromagnetic waves called terahertz (THz) waves have been an unexploited region until recently. This region almost coincides with the far-infrared region (Fig. 1) and is sometimes defined as the frequency region of 0.1∼10 THz (1 THz = $10^{12}$ Hz). 1 THz = 33.3 $cm^{-1}$ and corresponds to the wavelength of 330 μm. The technology of generating THz waves has made great progress recently after the invention of the method of generating THz broadband pulses using femtosecond lasers [1–3]. There are various characteristic excitations in a number of materials which can be probed by THz waves as shown in Table 1. This technique has started to be applied to various fields from basic science to industry (Fig. 2). Quite recently, THz spectroscopy has been applied to the measurement of the time evolution of discharge gas plasmas [4, 5] and dust forming plasmas [6].

In this paper, we review the recent development of THz techniques using femtosecond lasers intending to apply them to fusion plasma diagnostics in the future.

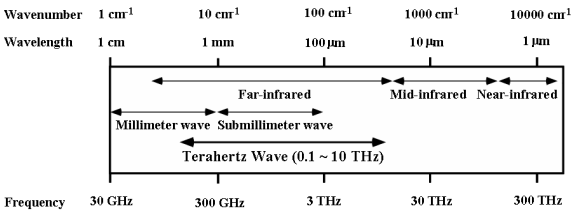


Fig. 1 Frequency range of THz waves.

Table 1 Various excitations in THz region.

| Material | Excitation |
|---|---|
| **Semiconductor** | **Free carrier, Phonon, Plasmon, LO phonon-plasmon coupled mode, Cyclotron resonance, Magnetoplasma** |
| **Ferroelectrics** | **Soft mode** |
| **Superconductor** | **Superconducting energy gap, Quasiparticle excitation, Intrinsic Josephson plasma, 2D-super carrier plasmon-polariton** |
| **Photonic crystal** | **Photonic band** |
| **Liquid** | **Relaxation mode** |
| **Gas** | **Rotational mode, Plasma** |
| **Biomolecule** | **Vibrational mode, Collective excitation related to biological function** |

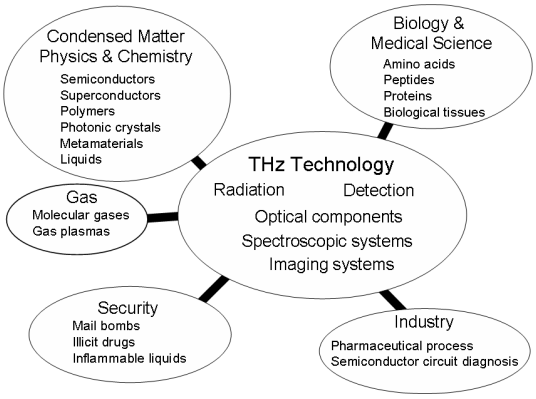


Fig. 2 Possible applications of THz technology.

## 2. Emission and Detection of THz Waves Using Femtosecond Lasers

THz radiation can be emitted from various materials and devices by exciting them with femtosecond lasers

*author's e-mail: hangyo@ile.osaka-u.ac.jp*

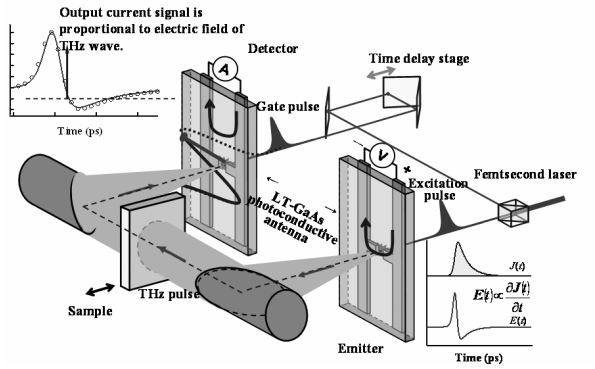


Fig. 3 Schematic diagram of THz emission and detection system.

[2, 3]. It is emitted from semiconductor photoconductive antennas (Auston switches), semiconductor surfaces, nonlinear optical crystals, superconducting devices and films, etc. The emitted THz radiation can be detected by the coherent detection method by gating the detecting devices (photoconductive antennas or electro-optic crystals) by femtosecond laser pulses. Here, we briefly explain the emission and detection methods of THz wave pulses by semiconductor photoconductive antennas.

Figure 3 shows the schematic diagram of emission and detection of THz waves by femtosecond laser pulses. The optical pulses (~800 nm wavelength, ~100 fs timewidth, and ~100 MHz repetition rate) are delivered from a femtosecond laser and focused on a photoconductive antenna. The photoconductive antenna is a thin film of a photoconductive semiconductor (low-temperature grown GaAs is frequently used) with electrodes having a small gap inbetween on a substrate. The electrode is voltage biased. A transient photocurrent flows in the gap with the irradiation of the femtosecond pulses and the THz pulses are emitted into free space. The detector is also a photoconductive antenna but connected to a current amplifier. The detector is triggered by gate pulses split from the main pulses and time-delayed with a delay circuit. The gate pulses hit the electrode gap of the detector photoconductive antenna and the generated photo carriers are accelerated by the electric field of the THz pulses. The output current is proportional to the electric field of the THz pulses. By scanning the optical delay, the wave forms of the THz waves are measured.

Figure 4 (a) shows the typical wave form of the THz pulse. It has a very narrow time width of 0.25 ps. Figure 4 (b) shows the power spectrum obtained by the Fourier transformation of the wave form in Fig. 4 (a). The spectrum extends from nearly 0 to 150 $cm^{-1}$ (4.5 THz).

## 3. THz Time-Domain Spectroscopy and Its Application to Solid State Plasmas

There is a unique THz spectroscopy using the method

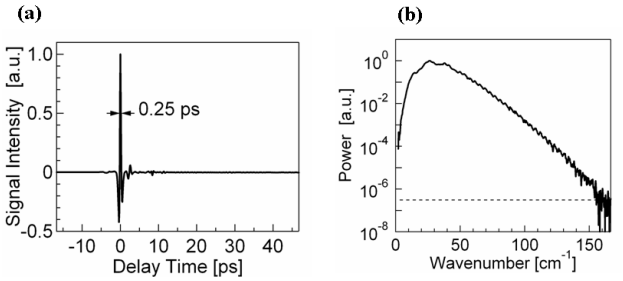


Fig. 4 (a) Typical THz wave form and (b) power spectrum.

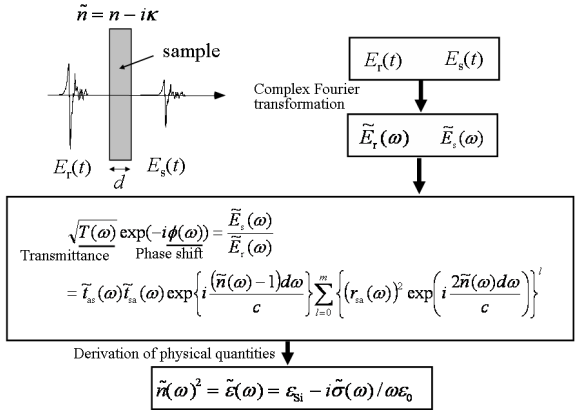


Fig. 5 Procedures for deducing complex optical constants from the measurement of THz wave forms.

of emission and detection of THz waves excited by femtosecond lasers [7, 8]. Since the wave form can be obtained by the system in Fig. 3, the real and imaginary parts of the optical constants (complex refractive index $\tilde{n} = n - i\kappa$, complex dielectric constant $\tilde{\varepsilon} = \varepsilon_1 - i\varepsilon_2$, complex electrical conductivity $\tilde{\sigma} = \sigma_1 - i\sigma_2$, etc.) are obtained at once by measuring the wave forms $E_r(t)$ and $E_s(t)$ with and without a sample as schematically described in Fig. 5. This spectroscopic method is called "THz time-domain spectroscopy (THz-TDS)". The sample is a plane-parallel plate. The complex transmission amplitude, which is described by the power transmittance $T$ and the phase shift $\phi$, is obtained by the complex Fourier transformation of the wave forms. Since $T$ and $\phi$ are functions of the complex refractive index, $n$ and $\kappa$ are obtained by solving the equation shown in Fig. 5. From $\tilde{n}$, $\tilde{\varepsilon}$ and $\tilde{\sigma}$ are obtained.

As a typical example, the results of a P-doped n-type Si wafer are shown in the following [9]. Figure 6 shows the temperature dependence of the THz wave form transmitted through the sample. The wave forms transmitted through the sample are delayed relative to the reference pulse with decrease in amplitude. The amplitude increases with decreasing temperature and the delayed pulse doubly reflected in the sample appears. Following the procedure in Fig. 5, the real and imaginary parts of the complex electrical conductivity are deduced as shown in Fig. 7. It is known that the electrical conductivity of doped Si is well

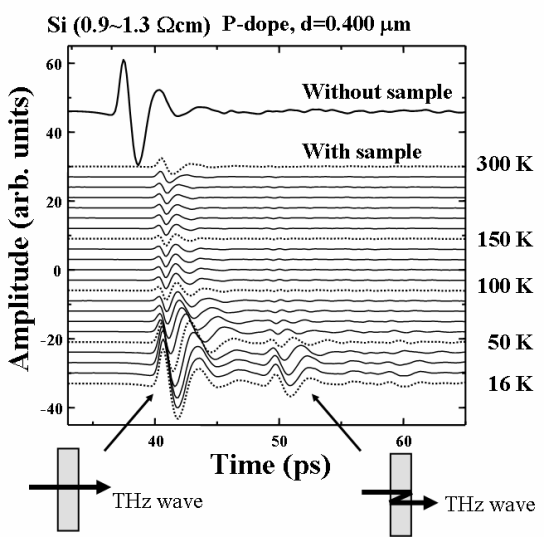


Fig. 6 Temperature dependence of the THz wave form transmitted through doped Si.

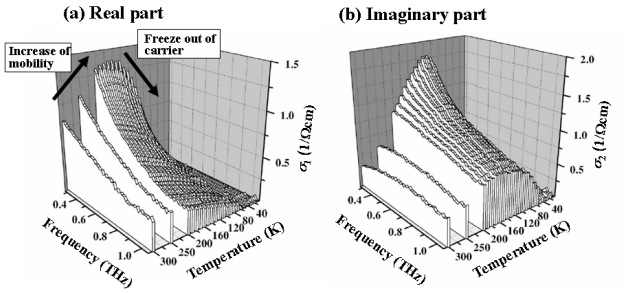


Fig. 7 Temperature dependence of (a) the real and (b) imaginary parts of the complex electrical conductivity of doped Si.

explained by the Drude model with the constant parameters, carrier density $n_e$ and collision rate $\gamma$ [10]. In this model, the complex conductivity at an angular frequency $\omega$ is given by

$$\tilde{\sigma}(\omega) = i\varepsilon_0\omega_p^2/(\omega + i\gamma),$$
$$\omega_p = \sqrt{n_e e^2/\varepsilon_0 m^*}. \quad (1)$$

where $m^*$, $\varepsilon_0$, and $e$ are the effective mass of the carrier, dielectric constant of vacuum, and electronic charge, respectively. By fitting the experimental data to the Drude model, the temperature dependence of the carrier density and mobility is obtained. This method is noncontacting and without magnetic fields, which is different from the Hall measurement, and a spatial resolution of ~1 mm is possible when the incident THz beam is well focused.

Next, we show an example of the measurement of the magneto-optical effect [11, 12]. The sample is the same as that used in Figs. 6 and 7. We specially designed and constructed a magneto-optical THz-TDS system using two closed-cycle He refrigerators (Gifford-McMahon refrigerators) for cooling a superconducting magnet and a sample

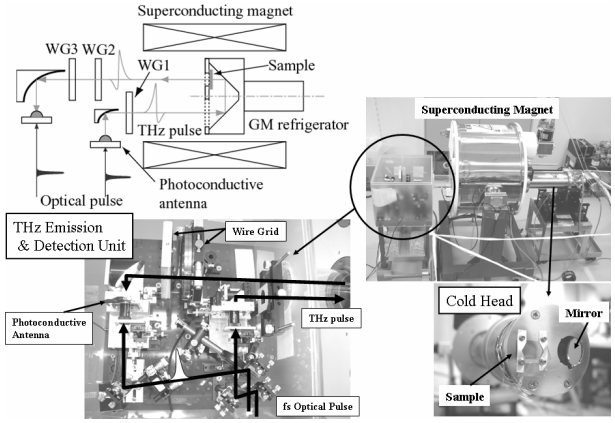


Fig. 8 Schematic diagram and photographs of the magneto-optical THz-TDS system.

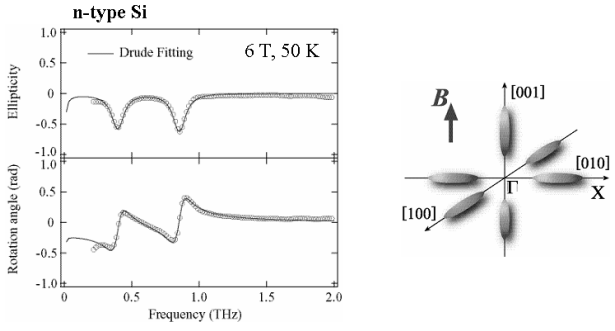


Fig. 9 Cyclotron resonance of doped Si.

as shown in Fig. 8. The generated THz pulse travels along the bore of the magnet and is reflected back by a V-shaped mirror on a cold stage of the refrigerator. The magnetic field is applied parallel to the THz beam (Faraday configuration). To avoid the influence of the mechanical oscillation of the refrigerators on the data, we monitored the oscillation by an acoustic sensor attached on the refrigerator for sample cooling and sampled the data synchronously with the acoustic signal. The wave forms were measured for two mutually orthogonal polarization directions. From the wave forms, the ellipticity and rotation angle of the polarization ellipsoid are deduced. Figure 9 shows the ellipticity and rotation angle spectra of the sample at 6 T and 50 K. Two clear dips of the ellipticity and dispersion in the rotation angle spectrum correspond to the cyclotron resonances for longitudinal and transverse effective mass carriers in the six valleys near the X points in the Brillouin zone. Both ellipticity and rotation angle spectra are well fitted by the Drude model. Such spectra can be obtained naturally by the THz-TDS method in contrast to the standard far-infrared Fourier transform spectroscopy, in which the tedious procedure of measuring the polarization property by rotating the polarizer is necessary.

The THz-TDS is also powerful for measuring the rotational transitions of gases [13, 14]. Figure 10 (a) shows the

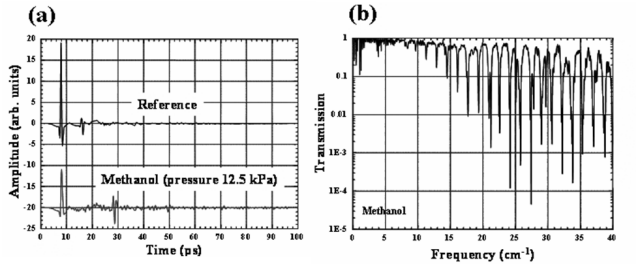


Fig. 10 (a) THz wave form and (b) transmission spectrum of methanol gas.

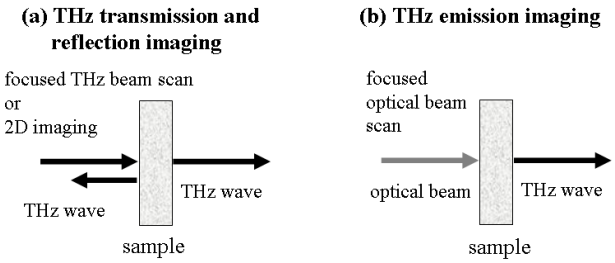


Fig. 11 Schematic illustrations of two types of THz imaging.

wave forms before and after the methanol gas is introduced in the sample cell. The wave form with the gas corresponds to the so-called free induction decay after passing of the incident THz wave pulses. Fig. 10 (b) shows the transmission spectrum corresponding to the rotational transitions obtained by the Fourier transformation of the wave forms in Fig. 10 (a). The THz-TDS is effective in identifying gas species.

Applications of the THz-TDS method to gas plasmas have just started quite recently by several groups. The transmission THz-TDS was applied to the characterization of discharge gas plasmas. From the delay time dependence of the transmitted THz wave form, the time evolution of the plasma parameters, i.e. the density and collision rate, has been deduced by the Drude model analysis as well as solid state plasmas [4, 5]. The THz-TDS was also applied to the detection of molecules in dust forming plasmas [6].

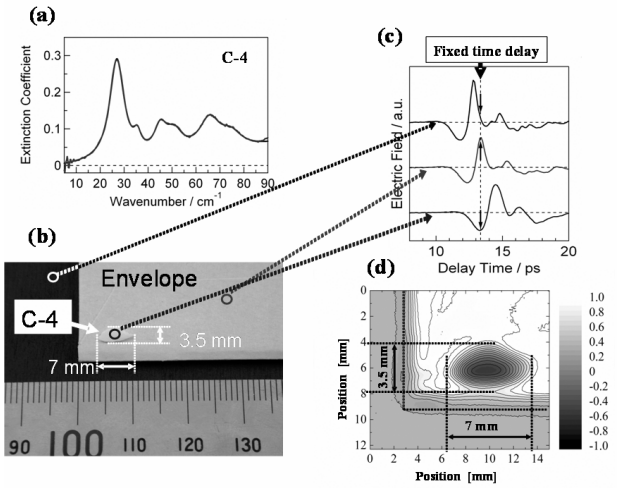


Fig. 12 (a) Absorption spectrum of the plastic bomb C-4 and (d) the THz image of a small piece of C-4 in the envelope. (b) and (c) indicates the correspondence of the wave forms and positions in the envelope.

## 4. THz Imaging

THz waves have unique transmission properties:

1) Plastics, papers, and ceramics transmit THz waves rather well.
2) Liquid water absorbs THz waves strongly.
3) THz waves are safe for human bodies in contrast to ionizing electromagnetic waves such as X rays.
4) THz waves are not transmitted for long distance in air.

Based on these properties, the THz imaging is expected to be used in various purposes [15, 16]. Here, we show some THz imaging systems and their applications. There are two types of imaging method as shown in Fig. 11 schematically. Fig. 11 (a) shows the conventional imaging method with a focused THz beam, where the transmission or reflection is measured with changing the focusing position in the plane perpendicular to the beam direction. The two-dimensional imaging with the combination of an electro-optic (EO) crystal and C-MOS or CCD camera has also been developed. The other imaging method called THz emission imaging shown in Fig. 11 (b) can be applied to samples which themselves are THz emitters excited by femtosecond laser pulses. By scanning the focused laser beam on the sample and detecting the THz waves, the THz emission image is obtained. The emission intensity image reflects the built-in electric field on semiconductor surfaces, voltage applied on integrated circuit, supercurrent density in superconductors, and so on depending on the emission mechanism.

Figure 12 (a) shows the absorption spectrum of a plastic bomb C-4 [17]. The spectrum has characteristic features. Plastic bombs in mails can be detected by the THz-TDS method since the paper is transparent to the THz waves. A small sample of C-4 in an envelope is placed at the focal point of the THz beam. By fixing the optical delay time and translating the sample two-dimensionally perpendicular to the beam direction, the image of the small piece of C-4 is obtained as shown in Fig. 12 (d).

The scanning type THz imager takes considerable time to obtain the two-dimensional image. Zhang and coworkers have proposed and demonstrated the real-time imaging system with the combination of the ZnTe EO crystal and the CCD camera [18]. Figure 13 shows the schematic diagram of the real-time two-dimensional imaging system using the ZnTe crystal and C-MOS camera developed by our group [19]. The amplified femtosecond laser is operated at 1 kHz. The intensity distribution in the beam of the probe pulse after transmission through the

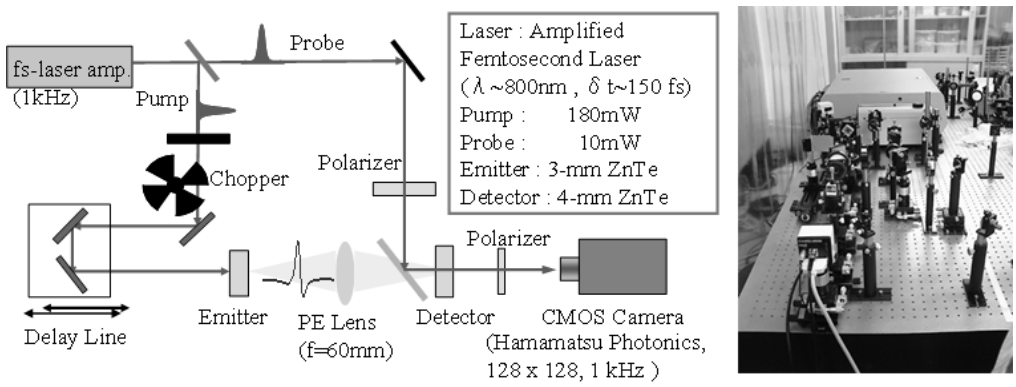


Fig. 13 Schematic diagram of the real-time THz imaging system.

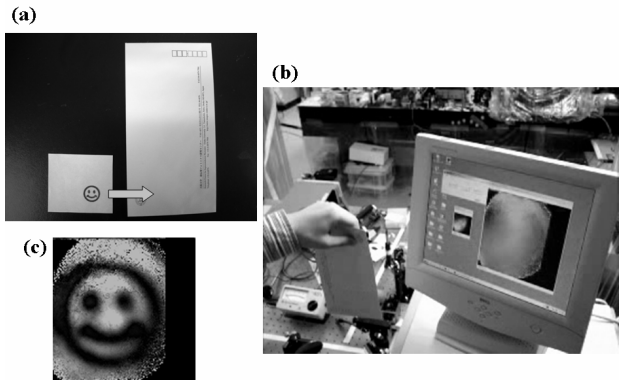


Fig. 14 Real-time THz imaging of the plastic sample in the envelope. (c) shows the THz image.

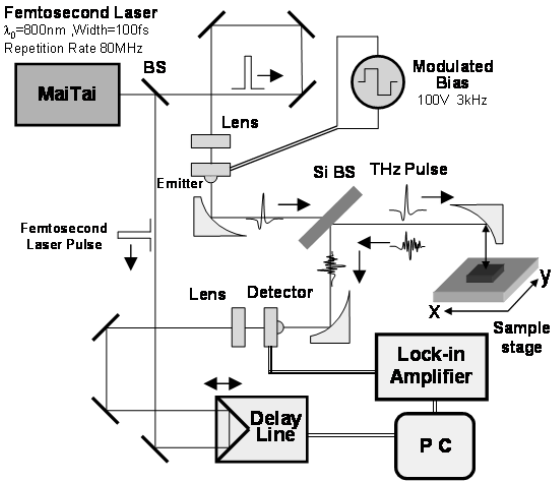


Fig. 15 Schematic diagram of the reflection-type THz imaging system.

ZnTe crystal is modulated spatially owing to the Pockels effect by the THz electric field and the THz image converted to the optical one is formed on the C-MOS camera. However owing to the imperfection of the ZnTe crystal, the inhomogeneous background appears even without the THz waves. Therefore, we chopped the femtosecond laser pulse exciting the THz emitter at 500 Hz, resulting in the successive series of probe pulses with and without modulation by the THz waves. With the real time subtraction of the signals with and without THz pulses in the C-MOS device, a clear image without a background due to the ZnTe inhomogeneity is obtained. Figure 14 shows the real time imaging experiment of a plastic sample put into an envelope.

The reflection imaging method is effective for investigating the inner structure of samples [20]. Since the THz waves are in the form of very short pulse and the wave forms can be detected in time domain, tomographic imaging is possible by using the emission and detection system in Fig. 15 like a supersonic echo imaging. Figure 16 shows the reflection image of a Japanese coin. Fig. 16 (b) shows the reflected wave forms at two different positions on the coin showing different arrival times of the reflected pulses. We translated the sample two-dimensionally and get wave forms at each point. Fig. 16 (c) shows the various kinds of images; images at various frequencies, amplitude image, and delay time image. The spatial resolution increases with increasing frequency. The time delay image reflects the surface structure of the coin directly.

The reflection imaging can be applied to the tomographic imaging of the surface of a human body. Unfortunately, the strong absorption due to liquid water prevents the THz waves from penetrating into the skin more than ~100 μm. However, the imaging of the nail is possible as shown in Fig. 17. The boundary between the nail and inner skin is clearly seen in this tomographic image.

## 5. Summary

Recent THz technologies using femtosecond lasers including spectroscopy and imaging are described. The THz-TDS is applied to the characterization of solid state plasmas in doped Si, which can be analyzed by the Drude model. The THz imaging is effective for detecting objects concealed in mails. The reflection imaging is effective in measuring the surface and inner structure of objects.

Until now, the main focus of THz applications has

been on solid materials. However, some groups have noticed the effectiveness of the THz-TDS and imaging in the diagnosis of gas plasmas. Currently, the millimeter wave reflectometry has been used for the diagnosis of fusion plasmas. However, much higher frequency electromagnetic waves are necessary for the diagnosis of fusion plasmas of ITER. One possible solution of this problem is to use pulsed THz waves excited by a femtosecond laser as pointed out by Vayakis *et al.* [21] and Tokuzawa *et al.* [22] The time delay of the THz pulse reflected by the plasma corresponds to the distribution of the electron density as shown in Fig. 18. However, the average intensity of the THz radiation excited by present femtosecond lasers is of the order of 10 μW, which may be insufficient to probe large scale plasmas for fusion. The deflection of reflected THz pulses will be also a severe problem because the detection area of the present photoconductive antenna is of the order of ~100 $\mu m^2$. A strong THz source excited by a high intensity laser and broad area detector will be needed for the practical use for the diagnosis of ITER plasmas.

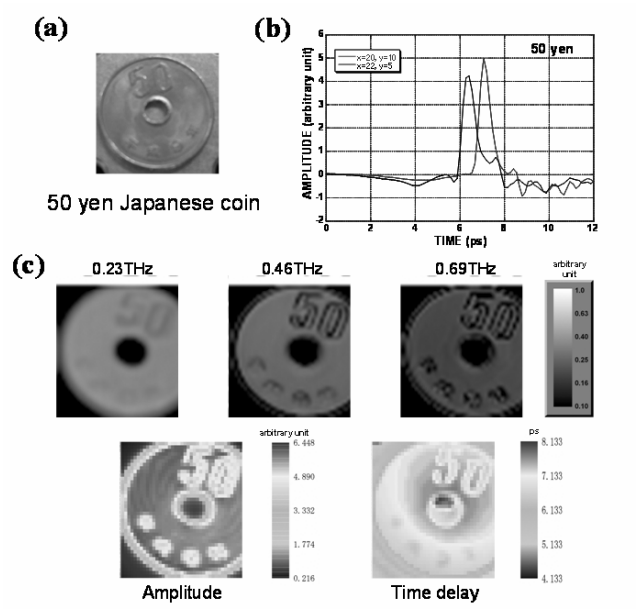


Fig. 16 Reflection images of the coin.

## Acknowledgments

This work has been supported partly by Terahertz Optics Project for Medical Application lead by J. Nishizawa, organized by Ministry of Education, Culture, Sports, Science and Technology, Japan. This work has also been supported partly by a Grant-in-Aid for Scientific Research from the Japan Society for the Promotion of Science.

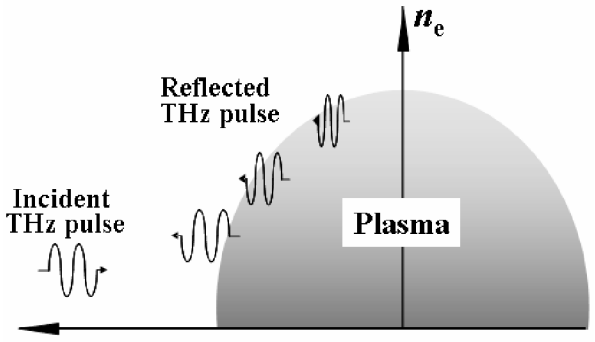


Fig. 18 Schematic illustration of fusion plasma diagnosis by THz wave pulses.

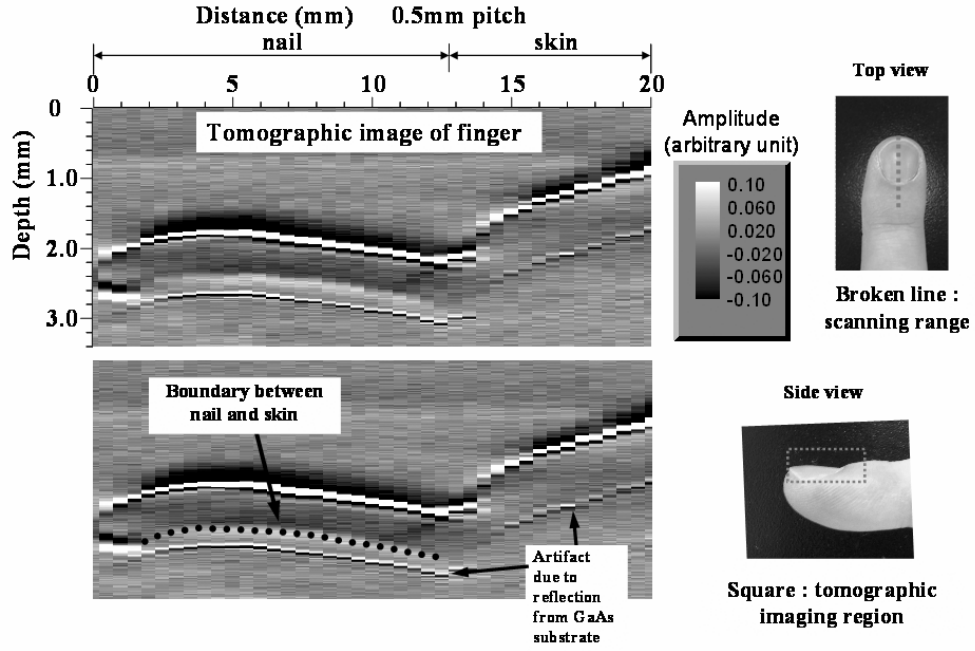


Fig. 17 THz tomographic image of the finger.

[1] D.H. Auston, K.P. Cheung and P.R. Smith, Appl. Phys. Lett. **45**, 284 (1984).
[2] *Sensing with Terahertz Radiation, edited by* D. Mittleman (Springer, Berlin, 2003).
[3] *Terahertz Optoelectronics, edited by* K. Sakai (Springer, Berlin, 2005).
[4] S.P. Jamison *et al.*, J. Appl. Phys. **93**, 4334 (2003).
[5] B.H. Kolner *et al.*, Appl. Phys. Lett. **87**, 151501 (2005).
[6] S. Ebbinghaus *et al.*, Plasma Sources Sci. Technol. **15**, 72 (2006).
[7] M. Hangyo, T. Nagashima and S. Nashima, Meas. Sci. Technol. **13**, 1727 (2002).
[8] M. Hangyo, M. Tani and T. Nagashima, Int. J. Infrared and Millimeter Waves **26**, 1661 (2005).
[9] S. Nashima *et al.*, J. Appl. Phys. **90**, 837 (2001).
[10] M. van Exter and D. Grischkowsky, Phys. Rev. B **41**, 12140 (1990).
[11] O. Morikawa *et al.*, J. Appl. Phys. **100**, 033105 (2006).
[12] H. Sumikura *et al.*, Jpn. J. Appl. Phys. **46** A,1739 (2007).
[13] M. van Exter, Ch. Fattinger and D. Grischkowsky, Opt. Lett. **14**, 1128 (1989).
[14] H. Harde, S. Keiding and D. Grischkowsky, Phys. Rev. Lett. **66**, 1834 (1991).
[15] B.B. Hu and M.C. Nuss, Opt. Lett. **20**, 1716 (1995).
[16] B. Feruguson and X.-C. Zhang, Nature Materials **1**, 26 (2002).
[17] K. Yamamoto *et al.*, Jpn. J. Appl. Phys. **43**, L414 (2004).
[18] Q. Wu, T.D. Hewitt and X.-C. Zhang, Appl. Phys. Lett. **69**, 1026 (1996).
[19] F. Miyamaru *et al.*, Jpn. J. Appl. Phys. **43**, L489 (2004).
[20] D.M. Mittleman *et al.*, Opt. Lett. **22**, 904 (1997).
[21] G. Vayakis *et al.*, Nucl. Fusion **46**, S836 (2006).
[22] T. Tokuzawa *et al.*, in *Abstracts of the 16th Int. Toki Conf.* (NIFS, Toki, 2006) P5-18, 86.